INSTITUT NATIONAL DE RECHERCHE EN INFORMATIQUE ET EN AUTOMATIQUE

Design of Minimal Dispersion Fluidic Channels in a CAD-Free Framework

Bijan Mohammadi J.I. Molho, J.A.Santiago

No 3982

July 2000

THÈME 4

ISSN 0249-6399 ISRN INRIA/RR--3982--FR+ENG

INRIA
ROCQUENCOURT

Design of Minimal Dispersion Fluidic Channels in a CAD-Free Framework

Bijan Mohammadi * J.I. Molho, J.A.Santiago †

Thème 4 — Simulation et optimisation
de systèmes complexes

Projet M3N

Rapport de recherche n ° 3982 — July 2000 — 21 pages

Abstract: We show the application of our shape optimization approach to the design of electroosmotic micro-fluidic channels realizing minimal geometrical dispersion on 90 and 180 degree turns. Our aim is to realize compact device of fluidic channels with maximum length in a minimum occupying surface. This means that we need to introduce turns along the channel. These turns, by modifying the electric field, introduce large skew and dispersion of the advected species which seriously degrades the detection and separation capacity of the ensemble.

Key-words: Fluidic Channels, Optimization, Incomplete Gradients, CAD-Free.

(Résumé : tsvp)

* Univ. Montpellier II and INRIA-M3N - e-mail: Bijan.Mohammadi@inria.fr
† Stanford Univ., Mech. Eng. Dept. Stanford, USA - e-mail: santiago@vonkarman.Stanford.edu

Unité de recherche INRIA Rocquencourt
Domaine de Voluceau, Rocquencourt, BP 105, 78153 LE CHESNAY Cedex (France)
Téléphone : 01 39 63 55 11 - International : +33 1 39 63 55 11
Télécopie : (33) 01 39 63 53 30 - International : +33 1 39 63 53 30

Conception de canaux fluidiques à dispersion minimale en environnement CAD-Free

Résumé : Nous montrons l'application de notre platforme d'optimisation pour la conception des canaux fluidiques à fonctionnement électroosmotique. Le but de ces configurations est la détection et la séparation de quantités microscopiques ayant des mobilités différentes lorsque suspendues dans un fluide et soumis à un champ électrique. Pour réaliser des configurations compactes de canaux, l'on est amené à introduire des coudes. Ceci implique, du fait de la variation du champ électrique, une grande dispersion des espéces transportées et nuit donc fortement aux capacités de séparation de l'ensemble. Le but est de proposer des formes minimisant cet effet et permettant ainsi la réalisation des canaux de longueur maximale sur une surface minimale et ayant la meilleure résolution possible. A cet effet, l'on considère deux types de coudes avec des angles de 90 et 180 degrés.

Mots-clé : Canaux Fluidiques, Optimisation, Gradients Incomplets, CAD-Free.

Contents

1 Introduction

Microfluidic channel systems used in bio-analytical applications are fabricated using technologies derived from microelectronics industry including lithography, wet etching and bonding of substrates. One important class of these channel system uses capillary zone electrophoresis to separate and detect chemical species. The aim is to analyze and then optimize the separation performance of such device for chemical tests. This technique separates chemical species suspended in a liquid buffer based on their electrophoretic mobility. The electric field in these systems is applied in the axis of the channel using electrode immersed at reservoirs at the end of the micro-channels. The ability to discriminate between sample species of nearly equal mobility is enhanced by increasing the channel length ([Culbeston, Jacobson & Ramsey (1998)], [Molho et al. (2000)]). Separation capacity increases with the length of the channel ([Culbeston, Jacobson & Ramsey (1998)], [Molho et al. (2000)]). In order to achieve channel lengths of order 1 m and yet confine the micro-channel system to a compact configuration with dimensions less than about 10 cm, curved channel geometries are required. Unfortunately, curved channel geometries introduce skews which imply a dispersion of the electrophoretic sample bands in the flow . This curved-channel dispersion has been identified as an important factor in the decrease of separation efficiency of electrophoretic micro-channel systems. Unfortunately, we notice that reducing the skew often introduce a new type of residual dispersion associated with band advection away from the channel boundaries. We also notice that to avoid this effect it is necessary for the channel walls to be as smooth as possible with minimal curvature variation. This is somehow contradictory with the shapes obtained from a minimization based only on skew minimization. We therefore add this constraint to our optimization.

The optimization formulation for such devices has to include therefore the following points:

- minimize the skew due to turns,
- minimize the residual dispersion associated with band advection,
- avoid too much variations in walls curvature,
- maximize the length of the channel,
- minimize the occupied surface.

Our aim in this paper is to show how to use our optimization platform, first designed for aeronautical applications ([Mohammadi (1997a)],[Mohammmadi & Pironneau (2000)]) to the design of minimal dispersion electrokinetic channels.

An important ingredient in the platform is the Computer-Aided-Design-free parameterization of the micro-fluidic channel geometry which has shown its ability to produce various new shapes not necessarily reachable in the original CAD parameterization. In this parameterization, the control space is quite rich compared to a CAD parameterization ([Mohammmadi & Pironneau (2000)]). We will see also that this parameterization enables to account for a possible loss of regularity in the manufacturing step.

Another important ingredient is to use dynamic minimization algorithms. We showed how to put well known minimization algorithms in the form of dynamic systems, having a decreasing energy like in Hamilton-Jacobi systems, suitable to reach stationary point for the solution of coupled problems. Indeed, in this approach, the minimization algorithm is seen as an extra state equation (for the parameterization) and the whole system is marched in a pseudo-time to a stationary point. Global minimization can also be introduced by coupling several dynamic systems from different parameterization states ([Mohammmadi & Pironneau (2000)]).

Finally, we would like to point out the issue of using incomplete sensitivities in the design process. The aim is to perform analysis and design at the same time. The main idea is to use two different state equations for the evaluation of the state variables and for the evaluation of sensitivities. The first one being usually complex and probably given by a commercial package, the second one simpler, but on which we have complete control and knowledge. The point being that we would like the simulation and design problems to have about the same complexity. We widely used this technique in shape design in aerodynamical applications ([Mohammmadi & Pironneau (2000)]) where the gradient of aerodynamical coefficients were approximated keeping only geometrical contributions ([Mohammadi (1997a)],[Mohammmadi & Pironneau (2000)]). This is especially important where the number of control parameters is large making otherwise necessary the use of an adjoint solver. This simplification is also important when the size of the direct simulation problem is quite what can be treated in a reasonable time by the existing computer facilities.

We show the application of this technique to the design of a 90 and 180 degrees corner minimizing the dispersion of chemical species in motion in the electric field. These turns are important as their combination permits to maximize the length to surface ratio for a channel. Typical cross-section sizes for these channels are 100 μm in cross-section width and 10 μm in depth.

2 Governing equations

This problem is multi-model in the sense that several PDE are involved in the definition of the state variables and the cost function. We will see that different levels of approximation can be introduced for these state equations.

2.1 Electric field

The aim is to use the difference in the mobility of the species in an electric field $E(t,x)$. E can be both stationary and unsteady. In this work, we consider only steady electric fields.

$E = \nabla v$ is defined solving a Poisson equation for the potential v:

$$-\Delta v = 0, \quad \text{in } \Omega \tag{1}$$

$$v(\Gamma_{in}) = v_1, \quad v(\Gamma_{out}) = v_2, \quad \frac{\partial v}{\partial n} = 0 \quad \text{on other boundaries.}$$

2.2 Flow motion

For typical electrokinetic microchannel applications the observed flow motion has a velocity of about $10^{-4}m/s - 10^{-3}m/s$, channel thickness of 100 μm and kinematic viscosity about $10^{-5}m^2s^{-1}$. This leads to Reynolds numbers ranging from 0.001 to 0.01. Due to spontaneous charge separation that occurs at the channel walls, there is formation of an electric double layer ([Probstein]). The typical size of this layer is a few nano meters. The stiffness of this electric double layer makes it hardly computable using classical numerical approaches applied to the Stokes model with a Lorentz force term. However, it is known that at the edge of the double layer the flow is parallel and directly proportional to the electric field. The first model describing the flow motion can be therefore the Stokes system with the previous condition as wall-function.

$$\frac{\partial U}{\partial t} - \mu \Delta U + \nabla p = 0, \quad \text{in the channel} \tag{2}$$

$$U = \mu_{ek} E \quad \text{on the inner and outer walls,}$$

$$-\mu \frac{\partial U}{\partial n} + p.n = 0 \quad \text{on in and outflow boundaries,}$$

where μ_{ek} is the electrokinetic mobility of the flow, μ the dynamical viscosity and n the unit external normal to the boundaries.

2.3 Reduced models for the flow

In the absence of a pressure gradient, the previous model reduces to two elliptic equations for the velocity components and states that the velocity vector is locally parallel to the walls and proportional to the local electric field $U = \mu_{ek} E\tilde{U}$ with $\tilde{U}$ obtained solving for $\tilde{U} = (\tilde{u}_1, \tilde{u}_2)$:

$$-\Delta \tilde{u}_1 = 0, \quad -\Delta \tilde{u}_2 = 0, \quad \text{in} \quad \Omega, \tag{3}$$

$$\tilde{U} = (\tilde{u}_1, \tilde{u}_2) = \tau = (\tau_1, \tau_2), \quad \text{on channel walls,} \quad \frac{\partial \tilde{U}}{\partial n} = 0 \quad \text{on other boundaries,}$$

where τ is the local unit tangent to channel walls. Noticing that the electric field itself is parallel to walls, this means that the velocity is everywhere parallel and proportional to the electric field:

$$U = \mu_{ek} E. \tag{4}$$

We use this former model in our optimization problem. In addition, this model is interesting for incomplete sensitivity evaluation (see below), where different models are used for the state and gradient computations. In other words, even when using more complex models, we should consider this model as the state equation to be taken into account for sensitivity evaluation.

2.4 Advection of species

The motion of a species a at infinite Peclet number by the velocity field U computed above is described by:

$$a_t(x,t) + U(x)\nabla a = 0, \quad \text{in } \Omega, \tag{5}$$

$$a(\Gamma_{inlet}) = \text{given}.$$

As we consider the velocity field defined by the stationary electric field, this step is therefore only a post-processing step and is devoted to the qualification of the skew.

3 Design problem formulation

We consider the following constrained minimization problem:

$$\min_{x(t)\in X} J(x, q(x), u(q,x)), \tag{6}$$

$$E(x, q(x), u(q,x)) = 0,$$

$$g_1(x) \leq 0, g_2(q(x)) \leq 0, \quad g_3(q, u(q,x)) \leq 0,$$

where $x \in X \subset R^{n_c}$ describe our CAD-Free parameterization ([Mohammadi (1997a)]). $q(x)$ describes all geometrical entities (normals, surfaces,...). $u \in R^N$ denotes the state variables (here the potential, electric field, fluid velocity and the advected species) and $E \in R^N$ the state equations described above. g_1 defines the constraints expressed directly on the parameterization and is taken into account in the definition of the admissible space X, g_2 those on geometrical quantities (for instance concerning the regularity of the shape) and g_3 state constraints on u (for instance concerning the regularity of the velocity field).

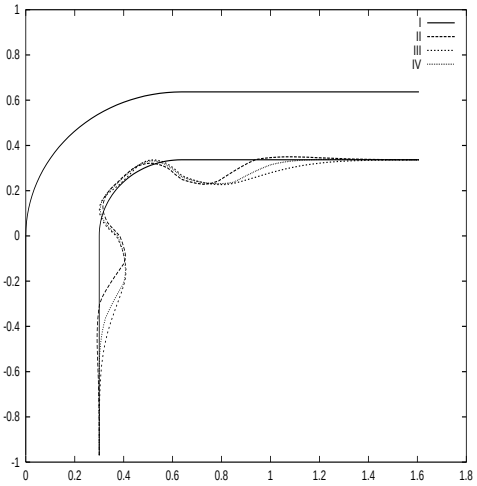

Figure 1: Shapes obtained under the same optimization conditions for three admissible spaces with different minimum required regularity for the shape.

3.1 Robustness

In many microfabricated fluidic channel systems ([Molho et al. (2000)]), it is difficult to exactly realize proposed shapes due to small but significant errors introduced in the manufacturing step. One way to account for these variations around to introduce a random perturbation operator in the optimization algorithm in the sense that the proposed shape is equivalent to any shapes in a given range (e.g. 5 percents in normal variation). The minimization problem (6) can therefore be reformulated as:

$$\min_{x(t)\in X} \max_{y\in Y(X)} J(y, q(y), u(q, y)), \tag{7}$$

with the state equation and constraints as above. Here the admissible space $Y(X)$ for the worst case analysis approach is defined by:

$$Y(X) = \{y \in [\frac{1}{\alpha}x, \alpha x], \forall x \in X\} \subset R^{n_c},$$

which for instance, for $\alpha = 1.05$ defines a 5 percent variation range around the proposed shape. If $\alpha = 1$, there is no randomness and the two optimization problems (6-7) are similar.

Another way to proceed is to perform the optimization in an admissible space with slightly less regularity requirement than what would be realizable by the manufacturing. Hence, the obtained shapes includes a possible imperfection. We propose the following approach:

- Define the admissible space X for the manufacturing,

- Extend X to X' including less regular shapes,
- Perform the optimization (6) in X',
- Project the optimized shape into X,
- Validate the regularized shape for the skew.

This approach is easy to account for in our CAD-Free parameterization presented bellow. We show in (Fig. 1) a possible loss of regularity for the shape during manufacturing, three designs have been performed under the same conditions but with slightly different minimum required regularity for the admissible spaces.

4 CAD-Free shape and mesh deformation tools

The shape deformation is done in a CAD-Free framework ([Mohammmadi & Pironneau (2000)]) in the sense that the only entity known during optimization is the mesh. This parameterization has several characteristics:

1. All the nodes on the inner wall of the channel are control points. More precisely, we use the local normal to the inner channel wall and specify the deformations in the direction of this normal $n(x)$. Hence, for a curve $\gamma(x)$, a deformation of amount $f(x)$, defined for each nodes, leading to the deformed curve $\tilde{\gamma}(x)$, can be expressed in the normal direction to γ by:

$$\tilde{\gamma}(x) = \gamma(x) + f(x)n(\gamma(x)).$$

2. To avoid oscillations, a 'local' smoothing operator is defined over the shape.

The reason for this is that the gradient has necessarily less regularity than the parameterization. Indeed, suppose that the cost function is a quadratic function of the parameterization: $J(x) = (Ax - b)^2$ with $x \in H^1(\Gamma)$, $A \in H^{-1}(\Gamma)$ and $b \in L^2(\Gamma)$. The gradient $J'_x = (2(Ax - b)A) \in V$ with $H^{-1}(\Gamma) \subset V \subset L^2(\Gamma)$. Hence, any parameterization variation using J'_x as descent direction will have less regularity than x: $\delta x = -\rho J'_x = -\rho(2(Ax - b)A) \in V$, where $H^{-1}(\Omega) \subset V \subset L^2(\Omega)$. We need therefore to project into $H^1(\Omega)$ using the localized solution of a second order elliptic system in regions where the deformation is found to be not enough smooth.

$$(I - \varepsilon\Delta)\delta\tilde{x} = \delta x, \tag{8}$$

$$\delta\tilde{x} = \delta x = 0 \quad \text{where constrained,}$$

where $\delta\tilde{x}$ is the smoothed shape variation for the shape nodes and δx is the variation given by the optimization tool. By 'local' we mean that if the predicted shape is locally

smooth, it remains unchanged during this step and ε is set to zero for these regions if,

$$\frac{\delta_{ij}(\delta x)}{(\delta x)_T} < TOL, \tag{9}$$

where $\delta_{ij}(\delta x)$ is the difference between the variations of the two nodes of each boundary edge and $(\delta x)_T$ the mean variation on this edge and TOL is a regularity tolerance factor.

Now, to include a loss of regularity as discussed above, it is sufficient to ask for more tolerance in the step above.

Once the shape deformation defined, it is propagated over the computational domain using elasticity based procedure as described in ([Mohammmadi & Pironneau (2000)]). These shape and mesh deformation tools have been used in optimization problems in 2 and 3D configurations for incompressible and compressible flows ([Mohammmadi & Pironneau (2000)]).

5 Cost function and constraints

We want to minimize the skew, which can be qualified in different ways. For example, we can ask for iso-values of the advected species to be always normal to the flow field. In this case, we can consider:

$$J(x) = \int_0^T \int_\Omega (\nabla a(x,t) \times U(x))^2 dx dt, \tag{10}$$

where T is the maximum migration time. These integrals are not suitable for cheap sensitivity evaluation as they involves information over the whole domain. In addition, this cost function is too restrictive as we are actually interested only in minimizing the final skew. The cost function reduces to:

$$J(x) = \int_\Omega (\nabla a(x,T) \times U(x))^2 dx, \tag{11}$$

which again reduces, in region of space where the channel has no turn and therefore where U is constant to:

$$J(x) = \int_\Omega (\frac{\partial a(x,T)}{\partial n})^2 dx, \tag{12}$$

where n is the normal direction to the local walls.

Another way to reduce the skew, which also avoids the previous restriction, is to ask for all particles traveling on characteristics to have the same migration time. Hence, the cost function is given by:

$$J(x) = (\int_\chi \frac{ds}{U} - \int_{\chi'} \frac{ds}{U})^2, \tag{13}$$

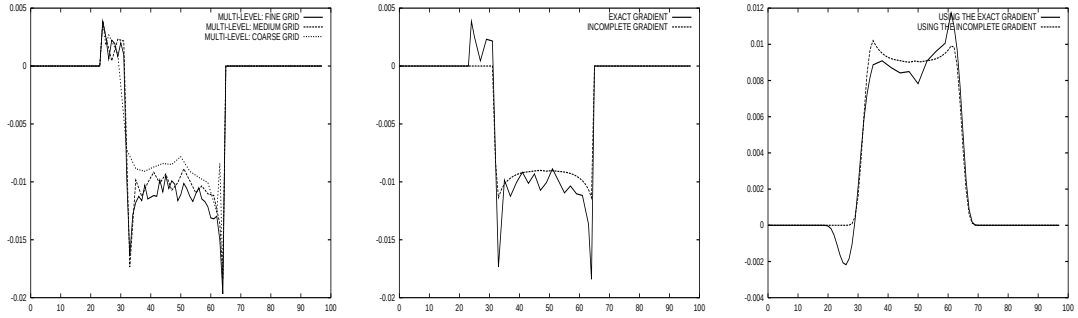

Figure 2: Sensitivity evaluation using the multi-level approach (left) for a initial 90 degrees corner. There are about 100 control points along the inner channel wall. Comparison between the exact and incomplete gradient evaluations (middle). The deformations obtained using the incomplete and exact gradients (right).

for any couple of characteristics χ and χ' linking the outlet to the inlet. Here again, the cost function is over the whole space, but we can consider only a few characteristics. The two main characteristics are those defined by the internal and external walls of the channel:

$$J(x) = (\int_{\Gamma_i} \frac{ds}{U.\tau} - \int_{\Gamma_o} \frac{ds}{U.\tau})^2. \tag{14}$$

where Γ_i is the inner wall and Γ_o the outer wall in a turn. This last formulation is interesting as it only involves boundaries which we know to be suitable for the application of our incomplete sensitivity. Another interesting feature of formulations (13 and 14) over (10) is that they do not require the knowledge of the distribution of the advected species.

As we said, we notice that the residual band advection dispersion away from walls increases with the variation of the shape curvature. We therefore add the following constraint to the cost function (14) above:

$$J(x) \leftarrow J(x) + (\int_{\Gamma_i} \|\frac{\partial n}{\partial s}\| - \int_{\Gamma_i^0} \|\frac{\partial n}{\partial s}\|)^2 + (\int_{\Gamma_o} \|\frac{\partial n}{\partial s}\| - \int_{\Gamma_o^0} \|\frac{\partial n}{\partial s}\|)^2, \tag{15}$$

where 0 denotes initial inner and outer walls. This is why, when we alow both walls to move, we obtain for about the same amount of skew, a higher residual dispersion inside the channel. In cases, where the outer wall is kept unchanged the second constraint vanishes.

Two other types of geometrical constraints concern the amplitude of the deformations and the regularity of the deformed shape. In the first constraint, shape variations are allowed between two limiting curves. Regularity requirements are enforced using the smoothing operator of the CAD-Free parameterization described above.

6 Sensitivity and incomplete sensitivities

Consider the general simulation loop, involved in (6), leading from shape parametrization to the cost function :

$$J(x) : x \rightarrow q(x) \rightarrow U(q(x)) \rightarrow J(x, q(x), U(q(x))).$$

The Jacobian of J is given by:

$$\frac{dJ}{dx} = \frac{\partial J}{\partial x} + \frac{\partial J}{\partial q}\frac{\partial q}{\partial x} + \frac{\partial J}{\partial U}\frac{\partial U}{\partial q}\frac{\partial q}{\partial x}.$$

In most applications, the cost function is, or can be reformulated, to have the following characteristics:

- The cost function J and the parameterization x are defined on the shape (or a same part of it),
- J is of the form

$$J(x) = \int_{\text{shape or part of the shape}} f(x, q)g(u)d\gamma,$$

  which means that it involves a product of geometrical and state based functions,

We have shown that for such cost functions, the sensitivity with respect to the state can be neglected in regions where the curvature of the shape is not too large ([Mohammadi (1997a)]-[Mohammadi (1999)]).

The concept of incomplete sensitivities was first introduced for aerodynamical applications involving hyperbolic and parabolic PDEs ([Mohammmadi & Pironneau (2000)]). In that work, we showed that where the cost function, constraints and controls are defined over the shape (through boundary integrals for instance), a good estimation of gradients are obtained by keeping only geometrical sensitivities. This means that only the shape deformation tool has to be differentiated and not the whole simulation loop, in particular neither the mesh deformation or the state equation solver have to be linearized ([Mohammadi (1997b)]). Hence, we consider the following approximation for the gradient:

$$\frac{dJ}{dx} \sim \frac{\partial J}{\partial x} + \frac{\partial J}{\partial q}\frac{\partial q}{\partial x}.$$

We can illustrate this idea on the following simple example. Consider as cost function $J = a^n u_x(a)$ and as state equation the following diffusion equation:

$$-u_{xx} = 1, \quad \text{on} \quad]\epsilon, 1[, \quad u(\epsilon) = 0, \quad u(1) = 0,$$

which has as solution $u(x) = -x^2/2+(\epsilon+1)/2-\epsilon/2$. We are in the domain of application of the incomplete sensitivities ([Mohammmadi & Pironneau (2000)]):

- the cost function is product of state and geometrical quantities (larger is n, better is the approximation),
- it is defined at the boundary,
- the curvature of the boundary is small (here no curvature at all).

The gradient of J with respect to ϵ is given by:

$$J_\epsilon(\epsilon) = \epsilon^{n-1}(nu_x(\epsilon) + \epsilon u_{x\epsilon}(\epsilon)) = \frac{\epsilon^{n-1}}{2}(-n(\epsilon+1) - \epsilon).$$

The second term between parenthesis is the state linearization contribution which is neglected in incomplete sensitivities. We can see that the sign of the gradient is always correct and the approximation is better for large n.

As we said, cost function (14) is suitable for the application of incomplete sensitivities. We can increase direct geometrical contributions by the fact that the velocity is parallel to the walls. The cost function we consider for derivation is therefore:

$$J(x) = (\int_{\Gamma_i} \frac{ds}{\vec{\tau}\mu_{ek}|E|} - \int_{\Gamma_o} \frac{ds}{\vec{\tau}\mu_{ek}|E|})^2., \tag{16}$$

where $\vec{\tau}$ is the local unit tangent vector to the wall.

To evaluate the accuracy of these gradients, we compare the results obtained with this approximation of the gradients with those coming from finite differences. This incomplete sensitivity evaluation possibility shows the importance of redefining cost functions as boundary integrals when possible (as shown above) and to bring as close as possible the cost function and control definition locations. This is in particular important for 3D configurations and it also permits to consider a whole circuit pattern and not only a piece of shape. In fact, optimization becomes possible for the configurations for which simulation is affordable as the cost of simulation and design becomes equivalent. Indeed, sensitivity analysis is now equivalent to the linearization of the following approximate simulation loop:

$$\tilde{J}(x) : x \to q(x)|_\Gamma \to J(x, q(x), U(q(x))),$$

which means that we only account for the modification in the geometrical part defined over the inner channel wall.

6.1 Multi-Level gradient construction

From what said on incomplete sensitivities, it is clear that it is more suitable to have an accurate state evaluation and an approximate gradient than to try to compute an accurate gradient based on a wrong state obtained on a coarse mesh.

Consider a bilinear cost function involving state u and geometrical q contribution and defined over the same region than the control x.

$$|\frac{d}{dx}(u.q) - u(\text{fine})\frac{dq}{dx}| < |\frac{d}{dx}(u.q) - \frac{du}{dx}(\text{coarse}).q + u(\text{coarse})\frac{dq}{dx}|.$$

The left hand side is the difference between exact and incomplete gradient computed on a fine mesh.

This error is often present and is due to the fact that the cost of iterative minimization and gradient evaluations limit the user to coarser meshes than what would have been used for a pure simulation.

One possibility to avoid this difficulty is to use different level of refinement for the state and the gradient. This is the idea behind multi-level shape optimization where the gradient is only computed on the coarse level of a multi-grid construction and where the state comes from the finer level ([Beux & Dervieux (1997)]):

$$\frac{d}{dx}(u.q)(\text{fine level}) = I(\frac{du}{dx}(\text{coarse level})).q(\text{fine}) + u(\text{fine level})\frac{dq}{dx}(\text{fine}).$$

The first term of the left hand side is the interpolation of the gradient computed on the coarse grid over the fine level.

7 Pseudo-unsteady closure equation for x

Consider the following time dependent equation for the shape parameterization x. Here, the time is fictitious and is similar to the descent parameter.

$$\dot{x} + \epsilon \ \ddot{x} = -F(\Pi, \mathcal{M}^{-1}, \nabla_x J).$$

F is function of the exact or incomplete gradient, it takes into account for the projection over the admissible space and the smoothing operator $(\Pi, \mathcal{M})$. This system represents most minimization algorithms. If $\epsilon = 0$, we recover the steepest descent approach. If $\epsilon > 0$, this is the heavy ball method ([Attouch & Cominetti (1996)]) The aim in this approach is to access different minima of the problem and not only the nearest local minimum. Conjugate gradient and quasi-Newton methods can also be cast in this form ([Mohammmadi & Pironneau (2000)]).

To advance in time (7), we use a central difference scheme (denotes by δx^p the shape deformation at step p):

$$(\frac{\epsilon}{\lambda^2} + \frac{1}{\lambda})\delta x^{p+1} = \frac{\epsilon}{\lambda^2}\delta x^p - F(\nabla_{x^p} J^p). \tag{17}$$

The shape parameterization x^0 being defined, the dynamical algorithm we use is as follows:

Optimization iterations

1. compute the gradient: $\frac{dJ^p}{dx}$ or $\frac{d\tilde{J}^p}{dx}$,
if ($\|\frac{d\tilde{J}^p}{dx}\| < TOL$ or $J^p < TOL$) stop.
2. define the new admissible shape deformation using (17):
δx^p, 3. smooth the deformations using (8),
4. deform the mesh.
5. compute the new state: u^{p+1}.
6. compute the new cost: J^{p+1}.
6. $p \leftarrow p+1$ and goto 1.

End of optimization loop.

8 Numerical results

In addition to the characteristics presented above, we use a Delaunay mesh adaptation technique by local metric control widely used in various simulations involving the solution of PDE's ([Frey & George (1999)], [Hecht & Mohammadi (2000)]). The impact of this coupling has been shown on a the advection of a passive scalar by the field (figures 3). It is clear that to have the same quality without mesh adaptation implies the use of a regular fine mesh everywhere, which is out of reach for general applications. The remeshing is also important and absolutely necessary as the large deformations introduced for the shape makes the mesh too distorted to be effective for finite element simulations.

We show the skews produced by 90 and 180 degrees turns in pictures (4-5). We then applied our optimization approach to these configurations. No symmetry assumption has been made. The first class of optimized shapes for the 90 and 180 degree turns (Fig. 6-7) correspond quite to what found by an intuitive design ([Molho et al. (2000)]). This is important as it permits some confidence on the global design approach. The second classes of optimized shapes for the 90 and 180 degree turns (Fig. 8-9) have been obtained asking for the cross-section not to reduce too much and also for less regularity for the shapes. But, this leads to more band dispersion away from walls. The previous optimization were performed under the constraint for the outer wall to remain unchanged. To avoid too much restriction in the channel cross-section, a third class of shape can be obtained asking for both the inner and outer walls to move (Fig. 10-11). However, this turn is may be not optimal neither as we would like also to avoid for two close 180 degree turns to interfere, which would imply a larger surface for the whole channel.

9 Concluding Remarks

We have shown how to combine incomplete sensitivity analysis and pseudo-unsteady optimization approach to design reduced dispersion electrophoretic microchannel devices.

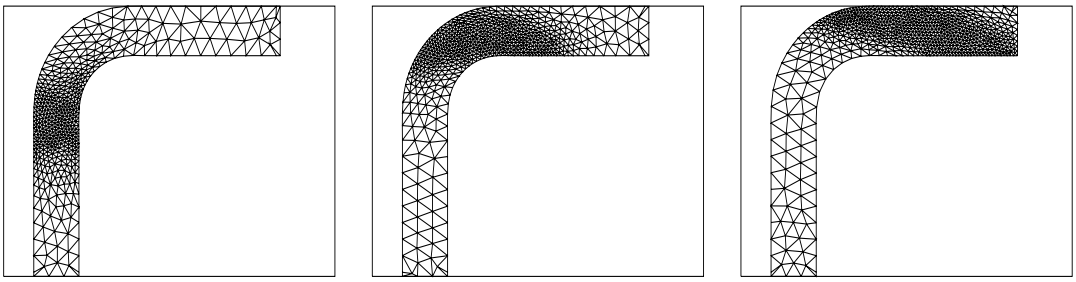

Figure 3: Adaptive simulation to capture accurately the skew.

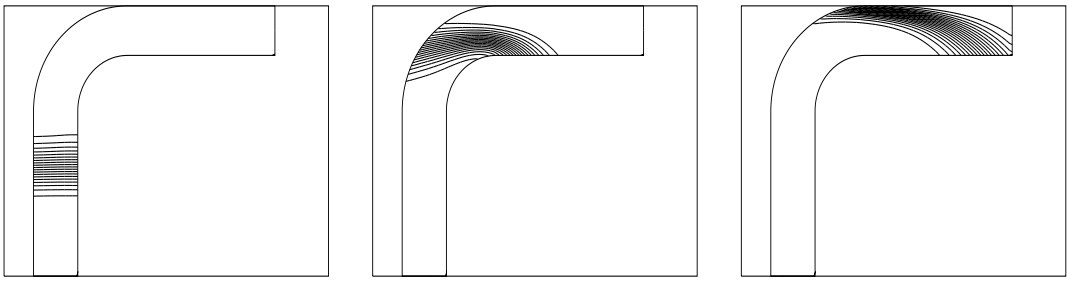

Figure 4: Initial shape for the 90 degrees turn: effect of the turn on the advected species.

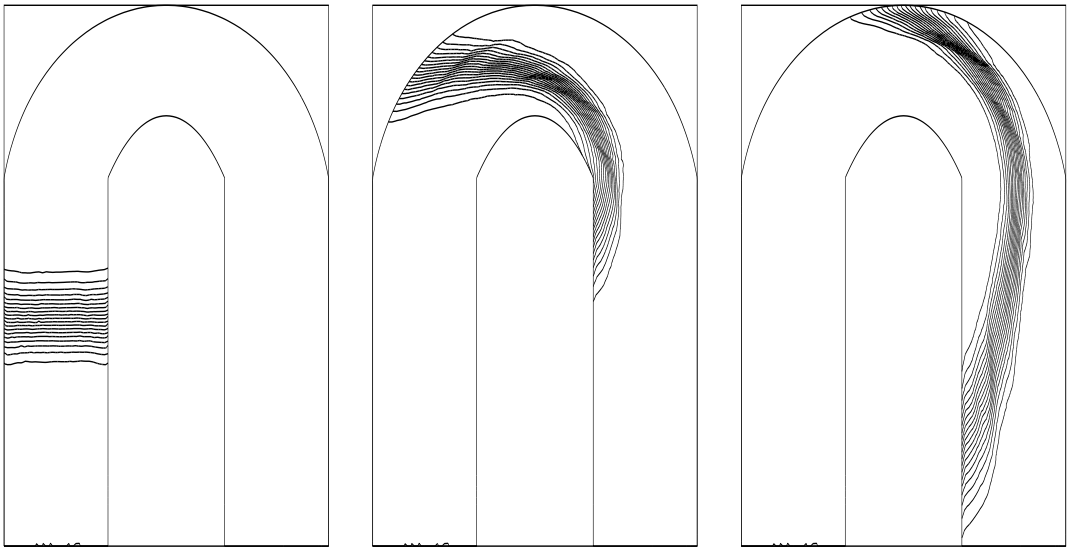

Figure 5: Initial shape for the 180 degrees turn: effect of the turn on the advected species.

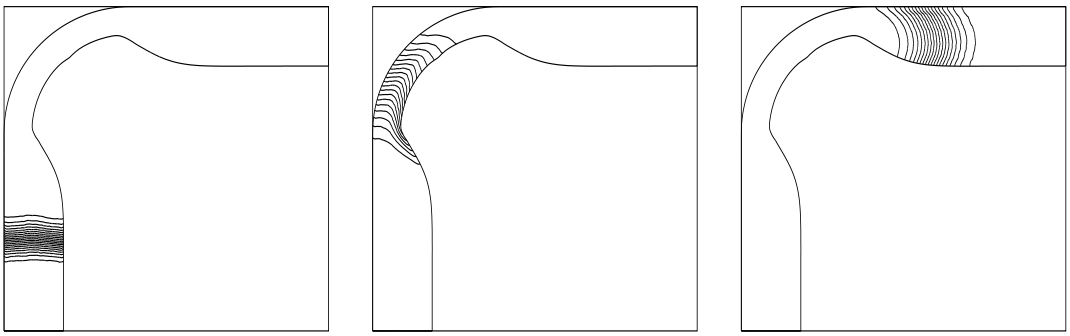

Figure 6: First class of optimized shapes for the 90 degree turn. The magnitude of the skew has been reduced by one order.

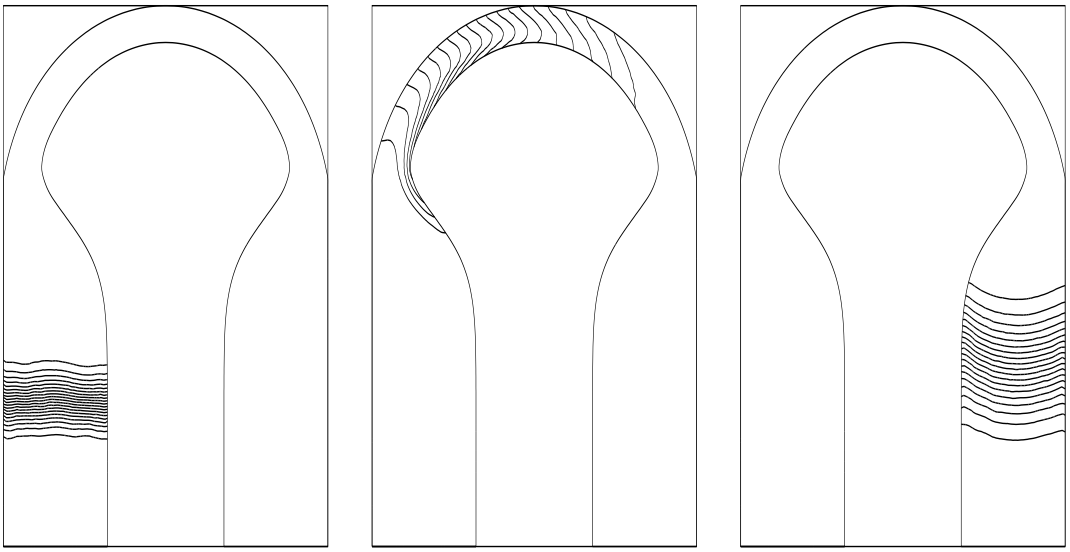

Figure 7: First class of optimized shapes for the 180 degree turn. The magnitude of the skew has been reduced by more than one order.

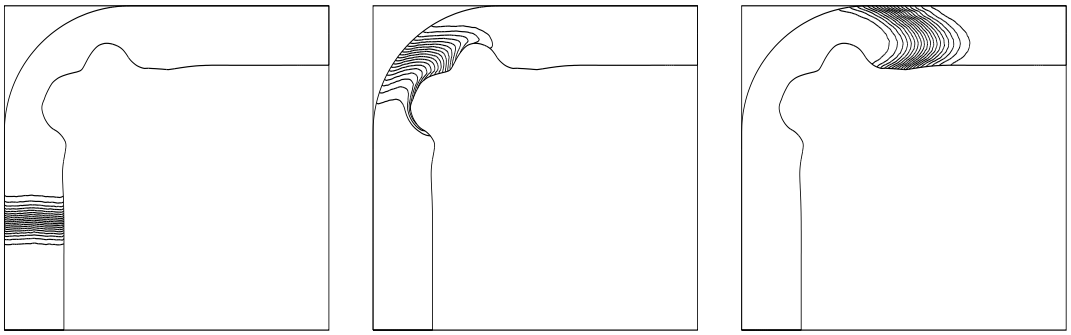

Figure 8: Second class of optimized shapes for the 90 degree turn. The magnitude of the skew is about the same than for the first class above with 15 percent less reduction in cross-section, but there is more dispersion in the advection band as the wall curvature variation is higgher.

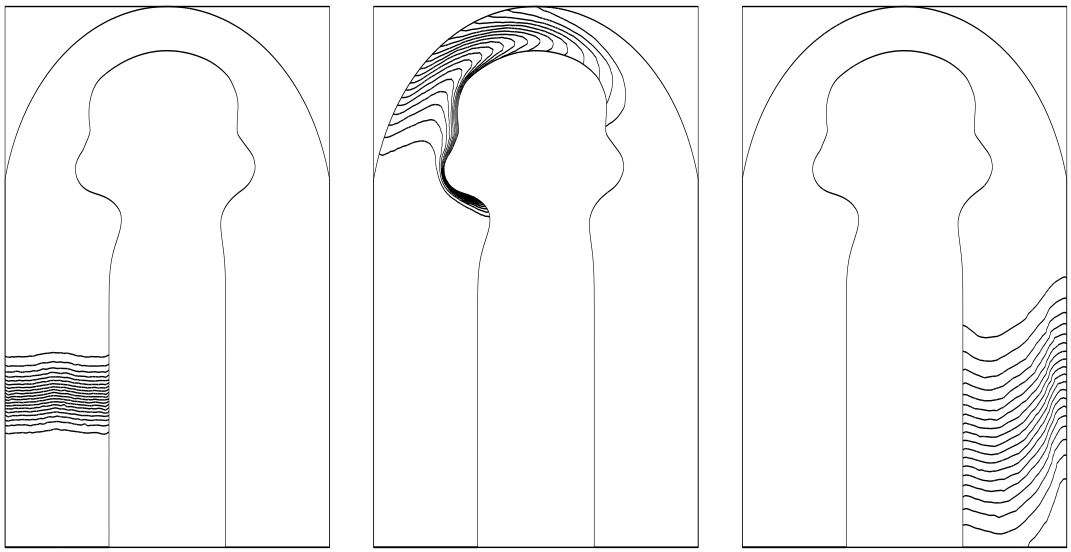

Figure 9: Second class of optimized shapes for the 180 degree turn. Here again, larger curvature variation introduces more dispersion in the advection band away from walls.

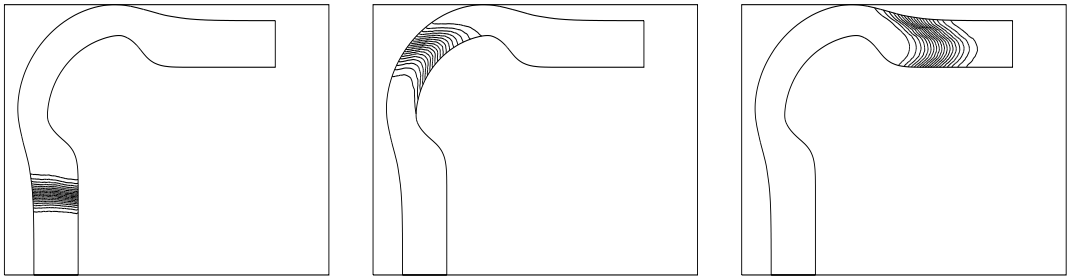

Figure 10: Third class of optimized shapes for the 90 degree turn with both the inner and outer walls moving. The skew is about the same than for the first class of the 90 degree optimized turn but with a much larger cross-section, but also more band dispersion away from walls.

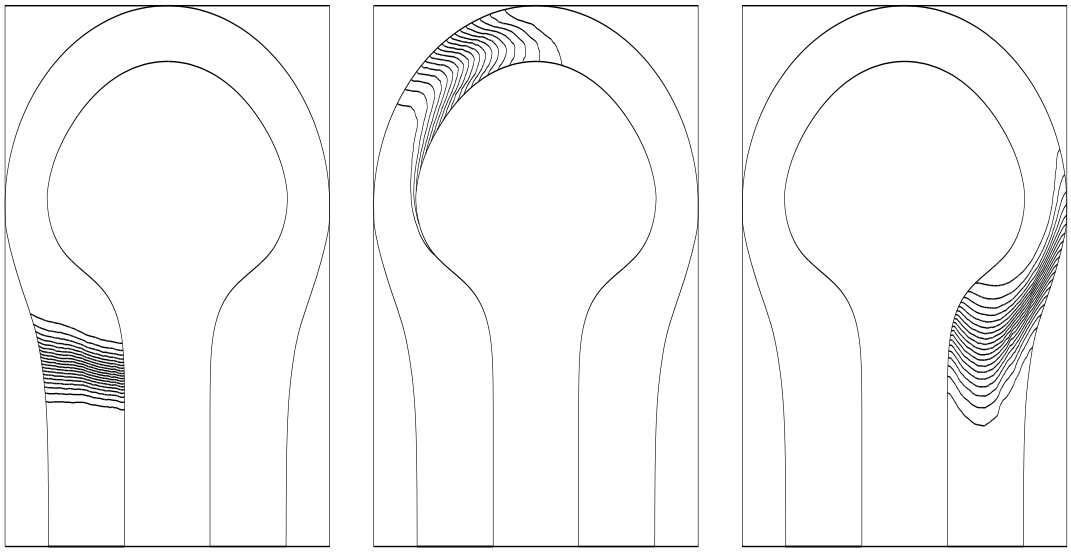

Figure 11: Third class of optimized shapes for the 180 degree turn with both the inner and outer walls moving. The skew has been quite reduced and the cross-section conserved (compared to the first class of shape), but there is much more band dispersion away from walls.

This analysis implies a redefinition of the cost function used for sensitivity evaluation based on approximate formula through boundary integrals. In addition, it has been shown that, to reduce the dispersion associated with band advection away from the channel walls, these walls need to be smooth with minimal curvature variation along the walls. Using the ingredients presented in this paper, minimal dispersion 90 and 180 degree turns have been obtained which enables by their combination to build low dispersion microfluidic patterns of any length in a minimum surface.

Acknowledgments

This work has been partly supported by the Center for Turbulence Research at Stanford university. Many thanks to prof. P. Moin, B. Perthame and O. Pironneau for their interests in this work realization. Many thanks to D. Spinks and M. Fatica for their permanent assistance during the summer institute.

References

[Culbeston, Jacobson & Ramsey (1998)] Culbeston C.T., Jacobson S. C.,Ramsey J. M. 1998 Dispersion Sources for Compact Geometries on Microchips, Analytical Chemistry, vol. 70, 3781-3789.

[Molho et al. (2000)] Molho J.I., Herr A.E., Mosier B.P., Santiago J.G., Kenny T.W., Brennen R.A., Gordon G.B. 2000 Designing Corner Compensation for Electrophoresis in Compact Geometries, proc. Micro Total Analysis Systems 2000.

[Mohammadi (1997a)] Mohammadi B. 1997,Practical Applications to Fluid Flows of Automatic Differentiation for Design Problems, VKI lecture series, 1997-05.

[Mohammadi (1997b)] Mohammadi B. 1997, A New Optimal Shape Design Procedure for Inviscid and Viscous Turbulent Flows, Int. J. for Numerical Meth. in Fluid, vol. 25, 183-203.

[Mohammmadi & Pironneau (2000)] Mohammadi B., Pironneau O. 2000, Applied Shape Design for Fluids, Oxford Univ. Press.

[Mohammadi (1999)] Mohammadi B. 1999, Flow Control and Shape Optimization in Aeroelastic Configurations, AIAA 99-0182.

[Probstein] Probstein R.F. 1995 Physicochemical Hydrodynamics, Wiley.

[Beux & Dervieux (1997)] Beux F., Dervieux A. 1997, A Hierarchical approach for shape optimisation , Inria report 1868.

[Attouch & Cominetti (1996)] ATTOUCH H., COMINETTI R. 1996, A Dynamical Approach to Convex Minimization Coupling Approximation with the Steepest Descent Method J. Diff. Eq., 128 (2) pp. 519-540.

[Frey & George (1999)] FREY P., GEORGE P.L. 1999, Maillages, Hermes.

[Hecht & Mohammadi (2000)] HECHT F., MOHAMMADI B. 2000 Mesh Adaptation for Time Dependent Simulation and Optimization, Revue Europèenne des Elements Finis, submitted.

Unité de recherche INRIA Lorraine, Technopôle de Nancy-Brabois, Campus scientifique,
615 rue du Jardin Botanique, BP 101, 54600 VILLERS LÈS NANCY
Unité de recherche INRIA Rennes, Irisa, Campus universitaire de Beaulieu, 35042 RENNES Cedex
Unité de recherche INRIA Rhône-Alpes, 655, avenue de l'Europe, 38330 MONTBONNOT ST MARTIN
Unité de recherche INRIA Rocquencourt, Domaine de Voluceau, Rocquencourt, BP 105, 78153 LE CHESNAY Cedex
Unité de recherche INRIA Sophia-Antipolis, 2004 route des Lucioles, BP 93, 06902 SOPHIA-ANTIPOLIS Cedex

Éditeur
INRIA, Domaine de Voluceau, Rocquencourt, BP 105, 78153 LE CHESNAY Cedex (France)
http://www.inria.fr
ISSN 0249-6399